The Large-scale Climate in Response to the Retreat of the West Antarctic Ice Sheet

F. Justino* and A. S. Silva†

Department of Agricultural Engineering , Universidade Federal de Viçosa, Brazil

M. P. Pereira

Department of Agricultural Engineering , Universidade Federal de Viçosa, Brazil

F. Stordal

Centre for Earth Evolution and Dynamics (CEED),

Department of Geosciences, University of Oslo, Norway

D. Lindemann

Department of Agricultural Engineering , Universidade Federal de Viçosa, Brazil

F. Kucharski

The Abdus Salam International Centre for Theoretical Physics, Trieste, Italy

Corresponding author address: Department of Agricultural Engineering , Universidade Federal de Viçosa, Brazil,

E-mail: fjustino@ufv.br

†Department of Agricultural Engineering , Universidade Federal de Viçosa, Brazil

ABSTRACT

Based upon coupled climate simulations driven by present day and conditions resembling the Marine Isotope Stage 31 (WICE-EXP), insofar the West Antarctic Ice Sheet (WAIS) configuration is concerned, we demonstrate that changes in the WAIS orography lead to noticiable changes in the oceanic and atmospheric circulations. Compared with the present day climate, the WICE-EXP is characterized by warmer conditions in the Southern Hemisphere (SH) by up to 5°C in the polar oceans and up to 2°C in the Northern Hemisphere (NH). These changes feed back on the atmospheric circulation weakening (strengthening) the extratropical westerlies in the SH (northern Atlantic). Calculations of the Southern Annular Mode (SAM) show that modification of the WAIS induces warmer conditions and a northward shift of the westerly flow, in particular there is a clear weakening of the polar jet. These changes lead to modification of the rate of deep water formation reducing the magnitude of the North Atlantic Deep Water, but enhancing the Antarctic Bottom Water. By evaluating the density flux we have found that the thermal density flux has played a main role in the modification of the meridional overturning circulation. Moreover, the climate anomalies between the WICE-EXP and the present day simulations resemble a bipolar seesaw pattern. These results are in good agreement with paleorecontructions in the framework of the Ocean Drilling and ANDRILL Programs.

1. Introduction

The large-scale Earth's topography has long been recognized to influence the climate system (Justino and Peltier (2006), Hamon et al. (2012), Kageyama and Valdes (2000)). For instance, the shape of the Antarctic ice sheet can potentially modify the stationary and transient atmospheric waves, the wind stress and thus the oceanic circulation (e.g. Justino et al. (2014), Knorr and Lohmann (2014)).

Past changes of continental and seaice from 65 to 1 Ma are primarily induced by changes in the configuration of the astronomical forcing (e.g. Scherer et al. (2008)). Recently, the influence of the atmospheric CO_2 concentration in leading the onset of the Antarctic glaciation has also been explored (DeConto and Pollard (2003)). DeConto et al. (2007) argued that once ice sheets are established, seasonal seaice distribution is highly sensitive to astronomical forcing and ice sheet geometry due to modification of the regional temperature and low-level winds.

As demonstrated by Zachos et al. (2001), the orography of the Antarctic ice sheet has changed substantially during the history of Earth. Lowering the Antarctic ice sheet height can result in a thermal forcing associated with the ascending lapse-rate inducing local warming (Justino et al. (2014)). Moreover, modification of the ice sheet mass balance leads to an anomalous pattern of the radiative balance due to changes in surface albedo (Pollard and DeConto (2005), Pekar and DeConto (2006), Pollard et al. (2005)). Of particular interest is the Marine Isotope Stage 31 (MIS31), that occured $\sim$ 1,08-1,07 Ma (million years ago, see Figure 1) in the early Pleistocene. This period is characterized by substancial deglaciation of the west Antarctica ice sheet (WAIS, Naish et al. (2009)). DeConto et al. (2012) using a 3-D ice sheet-shelf and global climate model to reconstruct the SST and seaice, have demonstrated a nearly complete collapse and subsequent recovery of marine ice in West Antarctica in the early Pleistocene.

These modelling results have been confirmed by The Ocean Driling Program (ODP) sites 1090 and 1165 showing that the MIS31 interval was considerably warmer than present. Additional support has been given by the marine glacial record of the AND-1B sediment core, recovered from the Ross ice shelf by the ANDRILL programme. Naish et al. (2009) have in particular documented astronomically-induced oscillations in the WAIS which collapsed at periodical intervals.

Previous investigations of the climate response to Antarctic ice sheet (AIS) variation have demonstrated that removal of the WAIS may increase the surface temperature by up to 4.9°C at DOME F and by up to 5.0°C at Dome C (Holden et al. (2010)). Goldner et al. (2013) evaluating the impact of adding an AIS to a "greenhouse world" mimicking the Eocene, and subtracting the AIS from the modern Antarctica, argued that the climatic feedbacks induced by the AIS did not lead to decreasing global mean surface temperature during the Eocene-Oligocene transition.

However, the authors demonstrated that the climate response due to the AIS changes is strongly modulated by the atmospheric CO_2 concentration. The climate response to modifications of the Antarctic topography has also been studied by Knorr and Lohmann (2014). In evaluating the role of an AIS expantion in the middle Miocene, it has been found that the ice sheet growth was accompanied by a warming in the surface waters of the SH Polar Ocean, which has been driven by atmosphere-ocean feedbacks on the initial wind field. Despite these efforts, the impact of distinct ice sheet configuration, such as during the MIS31 interval, on the wind driven and the thermohaline circulation (THC) has not been addressed in details.

To investigate the anomalous pattern of the austral seaice and SST DeConto et al. (2007) have applied the GENESIS climate model coupled to surface model components including a nondynamical 50-meter slab ocean. Although this modeling design has improved our understanding of coupled mechanisms of past climate change, it assumes a fixed deep-to-surface ocean heat flux. Thus, crucial ocean-atmosphere feedbacks that are important for the reorganization of the large-

scale climate are ignored. This limitation, however, can been overcome in coupled modelling studies using full ocean models. This also allows evaluation of changes in the THC, oceanic and atmospheric heat fluxes, and it provides a unique opportunity to study the influence of the WAIS in a global perspective. Moreover, the results can have relevance to both past interglacials when the WAIS retreated and potentially to future WAIS configurations.

2. Coupled climate simulations

In order to investigate the global climate response to retreat of WAIS resembling the WAIS conditions during the MIS31 interval (e.g. seaice, surface temperatures, the THC and oceanic and atmospheric heat fluxes), two model simulations have been performed with the Speedy-Ocean (SPEEDO) coupled model (Severijns and Hazeleger (2010)). A modern simulation driven by present day boundary conditions (MOD) and a second experiment that includes the ice sheet topography characteristic of the MIS31 interval (WICE-EXP). The MOD experiment has been described in detail in a previous publication (Justino et al. (2014)). The simulations (MOD and WICE-EXP) were run to equilibrium for 1000 years and the analyses discussed herein are based upon the last 50 years of each simulation.

The reason for performing a long numerical simulation is because of the need to reach a quasi-steady state. As stated in Danabasoglu et al. (1996) and according to their approach, the solution of the present study is defined by a quasi-steady state when the simulated seasonal and annual cycles become cyclic. This means that the analysed variables show little variation between cycles. The spin-up time for a given integration remains a topic of debate in the scientific community. Supposing that the interest is on oceanic equatorial surface fields, this spin-up time can be achieved with a few years of integration. However for mid-latitudes and deep waters, this time can be much longer, reaching decadal to centennial time scales.

The atmospheric component of the SPEEDO coupled model, called Simplified Parametrization, primitivE-Equation Dynamics (SPEEDY), is a hydrostatic spectral model with 8 vertical layers (925, 850, 700, 500, 300, 200, 100 and 30 hPa) and horizontal truncation T30, which corresponds to a horizontal resolution of 3.75°. It uses the divergence-vorticity equation. The oceanic component of the SPEEDO is the Coupled Large-Scale Ice-Ocean model (CLIO, Goosse and Fichefet (1999)). This model is based on the primitive equations (Navier Stokes equations) and uses free surface with a thermodynamic/dynamic parameterization of the seaice component. CLIO also employs a parameterization for vertical diffusivity, which is a simplification of the Mellor and Yamada turbulence scheme (Mellor and Yamada (1982)).

The ability of the SPEEDO model to reproduce basic features of the mean modern climate has been extensively analysed in Severijns and Hazeleger (2010). For example, the model is able to reproduce the large-scale mean flow in the Atlantic region and captures the South Atlantic Convergence Zone. The North Atlantic climatological atmospheric features, such as the mean and eddy geopotential height and the NAO variability of the atmospheric component of SPEEDO (SPEEDY), have been shown to compare well with present day observations (Kucharski et al. (2006)). The atmospheric climatology of SPEEDY is also systematically verified with respect to observations in `http://users.ictp.it/~kucharsk/speedy8_clim_v41.html`.

In order to further evaluate the reliability of SPEEDO to simulate the present day seasonal model variability, is shown in Figure 2 the first harmonic of precipitation, near air surface temperature and zonal winds, as well as in the NCEP/NCAR Reanalysis 1 (NNR1) and the Global Precipitation Climatology Project (GPCP). The first order harmonic of meteorological parameters shows long-term effects, while higher order harmonics show the effects of short-term fluctuations. The harmonic analysis is a useful tool to characterize different climate regimes and transition regions.

Moreover, it provides the possibility to identify dominant climate features in the space-time domain.

Figures 2a,d show higher seasonality over North America and northeastern Asia with values up to 30°C, a feature that is properly reproduced by the MOD simulation. Over the SH extratropics, both datasets agree on an enhanced seasonal cycle over South America, Africa and Australia, although over oceanic regions the SPEEDO simualtion displays weaker seasonality as compared with the NNR1.

Turning to precipitation (Fig. 2b,e), SPEEDO simulates a narrower band of precipitation in the tropical Atlantic region, thus, smaller amplitude of the seasonal cycle as compared with GPCP. It should be noted, however, that the MOD simulation reasonably reproduces the annual cycle of precipitation over the tropical forests of South America, Africa and Indonesia, as well as the precipitation pattern associated with moonsonal systems (e.g the Indian and South America monsoons). Evaluation of the zonal wind seasonal cycle demonstrates that the MOD simulation exhibits higher amplitude of the northeastern trade winds and the SH extratropical westerly flow compared to the NNR1. This deficience around Antarctica may very likely be due to an overestimation of the winter seaice area which can enhance the seasonal meridional thermal contrast. Elsewhere, the SPEEDO model can properly reproduce the seasonal fluctuation of the zonal atmospheric flow evident in the NNR1.

Figure 3a shows that in the zonal mean near surface temperature, SPEEDO compares well with the observed patterns. The largest difference between the model and the observations is located to the south of 75°S, where the steep topography of Antarctica plays a substantial role. This is a recurrent limitation in low resolution models as demonstrated by Justino et al. (2010). Several known problems have also being identified in the NNR1 in Antarctica as demonstrated by Chapman and Walsh (2007).

Analyses of precipitation (Fig. 3b) demonstrate that the MOD simulation is able to reproduce the most significant characteristics evident in the NNR1 data. The observed and simulated values over the equatorial regions associated with the Inter-Tropical Convergence Zone (ITCZ) exceed 6mm/day. The SPEEDO model can also reproduce the NH precipitation pattern in the storm track regions over the 40°-60°N latitudinal belt. Differences, however, between the simulated and NNR1 rainfall are found around 40°-60° in the Southern Hemisphere.

a. The WICE-EXP Simulation design

The ice sheet reconstruction characteristic of the MIS31 interval has been achieved by applying a combined ice sheet/ice shelf model, coupled to a high-resolution new treatment of grounding-line dynamics and ice-shelf buttressing to simulate Antarctic ice sheet variations over the past five million years (Fig. 1b, Pollard and DeConto (2009)). Figure 1c shows topography anomalies between these two simulations (WICE-EXP and MOD), that are by up to 2000m located in the current WAIS region. Elsewhere changes are smaller than 800m.

It is important to note that the inclusion of the MIS31 ice sheet topography (Fig. 1, Pollard and DeConto (2009)) leads to highly significant changes in the shape of the Antarctica ice sheet, with large ice free areas in west Antarctica. To include the effect of diabatic heating on the surface radiative balance the surface albedo is modified. In the MOD simulation the Antarctic ice sheet albedo is $\sim$ 70%, an intermediate value between the bare ice (54%) and snowfall (85%). In the WICE-EXP the albedo over ice free regions is computed by the oceanic model component. It should be noted that present time estimates of albedo based on observations in Antarctica are restricted to a few locations. Nevertheless, model estimates have proposed an ice sheet albedo varying from 70 to 85% (Munneke et al. (2011)).

Both simulations are run under atmospheric CO_2 concentration of 380 ppm and present day astronomical configuration. This allows for an isolated evaluation of the climatic effect associated with the WAIS collapse. It is important to notice that the MIS31 event experiment does not cover all aspects of this period. However, the sensitivity experiment can be applied to any "super-interglacial" of the early Pleistocene, or any of the periods in the Pliocene with a collapsed WAIS, when it comes to an investigation of changes in topography and albedo of the AIS.

b. Atmospheric circulation

The annual mean near surface air temperature (T2m) under present day conditions (Fig. 4a) exhibits the characteristic pattern with milder (warmer) temperatures over the extratropics (tropics), and lower temperature in the polar regions over Antarctica due to high continental elevation and the seaice effect. Turning to changes between the two simulations (MOD and WICE-EXP, Fig. 4b), it is evident that warming has occurred under WICE-EXP as compared with modern conditions. Furthermore, the SH warming also extends significantly northward over the tropical region and mid-latitudes, in particular over the western hemisphere. It should be noted that most changes in T2m are statistically significant at 95% level based on the t-test. Temperature differences over the western Antarctica, where changes in topography are largest, can reach values as high as 7°C (Fig. 4b). Over the eastern part of Antarctica lower temperatures are noted in the WICE-EXP by up to -5°C, compared to the MOD run. The simulated WICE-EXP warming/cooling over the ice cap is due to the combined direct and indirect influences of lapse-rate effect which follows changes in topography, in particular the collapse of the WAIS. This is opposite to what has occured during the Last Glacial Maximum (LGM), in the sense that during the LGM the WAIS was approximately 1000m higher than presently (e.g Whitehouse et al. (2012), Justino and Peltier (2006), Peltier (2004)). Interior ice elevations of the WAIS remains, however, uncentain. Ackert

et al. (2007) propose a WAIS approximately 125 m above the present surface during the 11.5 ka interval.

Over the polar oceans, anomalies are associated with enhanced warm advection from reduced WAIS and increased oceanic heat flux due to the substancial reductions in seaice thickness. It is important to note that the reduction in seaice area induces the albedo-seaice-ocean feedback leading to further warming. Over the mid-latitudes and tropics the WICE-EXP warming may be primarily related to weaker surface winds, and reduced evaporative cooling. It should be noted that colder conditions over the northern Atlantic are found in the region of deep water formation. This is in line with enhanced surface winds, as will be discussed later.

A brief comparison between the WICE-EXP results and the Pliocene Model Intercomparison Project (PlioMIP, Haywood et al. (2010)) demonstrates many similarities. For instance, Chan et al. (2011) and Haywood et al. (2009), based on OAGCM simulations, report higher zonal averaged air temperature at high latitudes by up to 5°C accompanied by a decrease in the equator-to-pole temperature gradient (Zhang et al. (2012). A large increase can be found in particular at polar latitudes. Indeed, this warming is a common feature in the PlioMIP: experimental design, mid-Pliocene boundary conditions and implementation special issue (`http://www.geosci-model-dev.net/special_issue5.html`).

In WICE-EXP the anomalous pattern of temperatures modifies the meridional thermal gradient and therefore the surface wind configuration. These changes in the thermal structure of the atmosphere are in accordance with the thermal wind relation which suggests a weakening of the westerly flow in the WICE-EXP simulation. The wind magnitude (Fig. 4d) reveals a substantial slowdown of the polar jet and the extratropical westerlies, however the sub-tropical jet has been strengthened around 30°S. This is particularly evident over the subtropical Atlantic ocean.

Turning to the Northern Hemisphere (NH), one may note an enhancement of the trade winds and the mid-latitude westerly flow which is clearly depicted over the Atlantic and Pacific basins. Hence, warmer air advection is expected to be intensified over Scandinavia and Eurasia leading to warmer temperatures in the WICE-EXP as compared with the MOD simulation (Fig. 4b).

Changes in temperature and surface winds are also associated with modification in the geopotential height at 700hPa (GH700, Fig. 4e,f). The main observed features of the present day stationary waves in the SH are reasonably reproduced in our MOD simulation. Despite the coarse spatial resolution of the SPEEDO atmospheric component, the model is able to reproduce the current low pressure system over the Ross and Amundsen-Bellingshausen seas (Hosking et al. (2013)).

The absence of the WAIS leads to highly significant changes in GH700 (Fig. 4f), in particular over the mainland of Antarctica and oceanic regions south of 50°S. This is primarily due to increased thickness of the column caused by enhanced lower tropospheric warming (Fig. 4b,f). Further analysis demonstrates that over the subtropical Atlantic ocean near the South America coast and around the 40°S latitudinal belt over Australia and the Pacific ocean, GH700 contracts so as to become of lesser extent as compared with modern conditions.

One should keep in mind that the substantial warming over west Antarctic in the WICE-EXP leads to distinct SH climate symmetry, which modified the spatial-temporal polar climate variability associated with the SAM, as will be discussed later. Justino and Peltier (2005) argued that the polar climate variability is strongly modulated by the direct mechanical effect of ice sheet topography (lapse rate), and by the effect of diabatic heating due to the marked change in the spatial variation of surface albedo.

The Z700 changes in the NH show an intensification of the Azores high and a deepening of the Icelandic low (Fig. 4f). This feature may indicate an intensification of the positive phase of the North Atlantic Oscillation (NAO). During the positive phase of the NAO, warmer condi-

tions are observed in Scandinavia that are accompanied by increased maritime air advection and strong westerly flow over the northern Atlantic. These patterns are well reproduced by the climate anomalies between the WICE-EXP and the MOD simulations.

The precipitation pattern depicted in the SH subtropics by the MOD simulation is primarily dominated in the Pacific and Indian Oceans by the influence of the recurrent baroclinic systems (Fig. 4g). In South America the precipitation band is primarily associated with the South Atlantic Convergence Zone (Fig. 4g). Also evident is the precipitation in the storm track region of the north Atlantic and Pacific.

In comparison with the MOD simulation, the WICE-EXP shows a decrease in precipitation in the tropical oceans, except over the Pacific (Fig. 4h). Positive anomalies are noted in the subtropics in the SH which are statistically significant. It is interesting to stress that the subtropical region experiences a substantial increase in precipitation related to the northward displacent of the main baroclinic zone due to changes in the meridional thermal gradient. These areas are also placed in good agreement with areas with reduced GH700 (Fig. 4f). Changes in the NH are weaker, although increased precipitation is evident in the northern Atlantic storm track region and in eastern Asia/ Pacific.

c. Southern Annular Mode

Based upon comparison of the MOD and WICE-EXP climates, in what follows the impact of these differences upon the spatial structure of the Southern Annular Mode (SAM) and its related features are investigated. SAM is responsible for the migration of the subtropical upper-level jet and variations in the intensity of the polar jet (Carvalho et al. (2005)), as well as for the intensification of an upper-level anticyclonic anomaly, weakened moisture convergence, and decreased precipitation over southeastern South America. Empirical orthogonal function (EOF) analysis has

been performed on Z700 monthly data throughout the 50 years of each model experiment. SAM is displayed in terms of the spatial pattern of its amplitude (Fig. 5), obtained by regressing the hemispheric Z700 anomalies upon the monthly leading principal component (PC) time series.

The leading pattern of variability in the MOD simulation (Fig. 5a) is characterized by an annular structure over the entire hemisphere which is dominated by two areas of strong out-of-phase variability located over mid-latitudes (40°-55°S) and the polar region (Fig. 5a). Although differences may be identified between our modeled SAM and the SAM resulting from climate system models of higher complexity (e.g Justino and Peltier (2006), L'Heureux and Thompson (2006)), it is evident that the SPEEDO provides a reasonable depiction of this atmospheric mode, characteristic wave number 3 . The first modeled EOF accounts for 54% of the total variance and is well separated from the second EOF which explains 6%. The temperature response to SAM is shown in Figure 5b. Fluctuations of SAM lead, during the positive phase, to slightly warmer near surface (colder) conditions in the subtropical (polar) region. This warming is evident in the southern Atlantic and southern South America regions and over the Antarctic peninsula, over Australia and the Tasman Sea, and southern Africa. It should be emphasized that during the positive phase of SAM our MOD simulation predominantly indicates positive near surface temperature anomalies globally (Fig. 5b). These characteristics are accompanied by weaker (stronger) westerlies in the vicinity of 30°S - 45°S (45° - 60°S, Fig. 5c).

Figure 5d shows the differences between SAM (first EOF of Z700) as a result of modification in the WAIS structure along with the modeled present day SAM. It should be noted that SAM in the WICE-EXP is no longer characterized by a predominant dipolar structure and it explains 48% of the climate variability, i.e lower variance as compared with the present day SAM. For instance, meridional changes in Z700 between the polar and extratropical regions in the MOD simulation may reach values up to 70 hPa, whereas in the WICE-EXP values do not exceed 30

hPa. Moreover, the well defined high pressures centres under MOD conditions are much weaker in the WAIS collapsed situation (Fig. 5d).

However, the southern Atlantic anticyclone is intensified which may increase the oceanic moisture advection to the subtropical part of South America (Fig. 5d). It should be noted, moreover, that the strengthening of this mid-latitude center of action in the WICE-EXP reduces the migration of colder extratropical air masses, creating a blocking situation. This further reduces the seasonal climate variability in South America/southern Atlantic. The opposite is found over southern Africa/Indian ocean and subtropical Pacific (Fig. 5d). Carvalho et al. (2005) discussed the degree of involvement of the seasonal subtropical climate and SAM, and the existence of strong teleconnection between the polar and subtropical regions in the SH has been demonstrated.

SAM-induced modification of the near surface temperature by changes in the WAIS (Fig. 5e) shows strong warming over the Antarctica peninsula/Belinghausen sea as well as over the polar ocean between 0-150°E. Over the eastern hemisphere, this clearly reflects the weakening of the SAM in the WICE-EXP. However, over the western hemisphere including the Antarctica peninsula, this cannot be assumed because SAM is no longer characterized by the annular structure. In terms of changes in the zonal wind, we found negative (positive) anomalies in the polar region (subtropics) and intensified wind curl in the WICE-EXP, as compared with the present day simulation (Fig. 5f).

These climate anomalies between the MOD and the WICE-EXP experiments and the differences between the climate response to SAM in the two simulations, reveal that despite the small area of the WAIS compared with the entire Antarctica, it plays a prominent role in setting up the SH atmospheric conditions.

d. Oceanic conditions

In what follows is discussed the role of the WAIS topography upon the oceanic conditions. Despite the low resolution of our oceanic component, the coupled model is able to simulate the intensified SST meridional thermal contrast (cold tongue) along the western coastal margins of South America as well as the coastal upwelling in Africa (Fig. 6a). It should be noted that a thorough evaluation of the present climate has been provided by Justino et al. (2014) and Severijns and Hazeleger (2010). As should be expected, changes in SST exhibit many similarities with the near surface air temperature anomalies (Figs. 4b, 6a), in particular in the extratropical region.

It is interesting to note that compared with the MOD simulation, WICE-EXP shows warmer conditions primarily confined in the SH. However, the warming along the latitudinal belt between 30-60°S shows values as high as 4°C in the southern Atlantic. Lower SSTs up to -2°C are found in the northern Pacific and Atlantic. This SST anomalous pattern resembles the oceanic response to increased freshwater into the northern Atlantic during the last glacial cycle (e.g. Rahmstorf (1996), Manabe and Stouffer (1995), Knutti et al. (2004)). These investigations suggested that changes in the rate of deep water formation and subsequently the reduction in the meridional oceanic heat transport was the primary contributor to the existence of the bipolar seesaw (Broecker (1998)). This assumption is further analysed in our study.

Figure 6c shows the present day seaice as simulated by the MOD run. Sea ice has a direct impact on the radiation budget of the climate system by affecting the net incoming solar radiation due to its high albedo (i.e. decreasing the absorption of solar radiation). Therefore, modification of the seaice cover may induce warming/cooling due to the seaice albedo feedback. As compared with satellite data, Severijns and Hazeleger (2010) argued that the seaice representation in

SPEEDO yields understimation of seaice in late summer and overstimation in late winter in both hemispheres.

Present day seaice thickness can reach values in the SH by up to 1m in the Weddell Sea and up to 1.2m in the Arctic ocean (Fig. 6c). Figure 6d shows that changes in the WAIS lead to substantiual reduction in the seaice thickness in both hemispheres. This is more evident in the Weddell and Bellingshausen seas, where atmospheric induced SST anomalies are the primary candidate to impose these changes. The importance of the wind field for leading changes in seaice has been explored by Lefebvre et al. (2004).

Figures 6e and 6f show the vertical distribution of zonally averaged ocean temperature anomalies, globally (Fig. 6e) and for the Atlantic basin (Fig. 6f). Globally the ocean temperature shows an averall warming from 60°S to 50°N in the WICE-EXP in comparison with the MOD simulation, which is more pronounced in the Southern Hemisphere down to 1000m depth. However, underneath this level lower temperatures are simulated in the WICE-EXP as compared with the MOD run.

In the Atlantic sector there has been an oceanic warming down to 1500m with values as high as 4.5°C. Below 1500m the ocean temperatures are much lower than the global average in the Atlantic. Marshall and Speer (2012) also argue that warmer surface conditions in the vicinity of the Antarctic continent may be related to water supplied from deeper layers along inclined outcropping density surfaces.

This vertical distribution of temperature may modify deep convection in the main sites of deep water formation. Indeed, this has been found to be the case. Figure 7 shows the anomalous pattern of the Meridional Overturning Circulation (MOC) as delivered by the WICE-EXP simulation. These results have demonstrated that the absence of the WAIS produces a remarkable weakening in the southward flow of the MOC (i.e North Atlantic Deep Water, NADW), as compared with

present day conditions. It is also evident (Fig. 7 top) that the northward returning flow (e.g. Antarctic Bottom Water, AABW) is intensified in the interior ocean. One may argue that this oceanic feature may be related to increased loss of heat to the atmosphere in the SH polar ocean and therefore enhanced downwelling.

It should be stressed that an additional contribution to this anomalous MOC in the WICE-EXP simulation, in particular in the SH, may arise from an anomalous Deacon cell which is primarily linked to the westward atmospheric flow (Marshall and Speer (2012), Speer et al. (2000)) .

To further investigate these changes we have computed the annual density flux as proposed by Schmitt et al. (1989) and Speer and Tziperman (1992). The surface density anomalies (a combination of the thermal and the haline density anomalies) have the potential to generate thermohaline circulation changes. To evaluate the thermal and haline contributions to the density changes in WICE-EXP, the thermal and haline components of the density flux ($kgm^{-2}s^{-1}$, Fig. 7a,b) are computed. The surface density flux based on Schmitt et al. (1989),

$$F_\rho = \alpha F_t + \beta F_S = -\alpha \frac{Q}{C_P} + \beta \rho \frac{(E-P-R-I)S}{1-S}, \tag{1}$$

includes the thermal expansion ($\alpha = -\frac{1}{\rho}\frac{\partial \rho}{\partial T} \mid_{p,S}$) and the haline contraction coefficient ($\beta = \frac{1}{\rho}\frac{\partial \rho}{\partial S} \mid_{p,T}$). In these expressions, $C_P, \rho_{(S,T)}, p, T$ and S are specific heat, density, pressure, sea surface temperature and salinity, respectively. Q, E, P, R and I represent net heat flux, evaporation, precipitation, runoff and water flux by sea-ice melting and growth, respectively.

In the northern Hemisphere (not shown) there are two regions of strong density gain; in the western North Atlantic, where cold and dry continental air masses blow onto relatively warm waters of the Gulf Stream and North Atlantic Current. The second region of density gain is in the Nordic Seas, due to a negative net heat flux associated to strong cooling of surface waters.

The contribution of the haline density flux to the total density is much smaller. However, it may dominate the density gain at the ice/water interface.

Figure 7 shows the surface density flux for MOD and the anomalies between WICE-EXP and MOD. Under present day conditions the region of strongest density gain is located in the Antarctic continental margins, in particular in the Ross and Bellingshausen Seas (Fig. 7a,b). This is primarily associated with the dominance of cold air embbeded in the westerly flow and due to the influence of katabatic winds. The second region of density gain is the southern Atlantic, where the model experiences a negative net heat flux associated with strong cooling of surface waters. The areas of density loss around the 30°-60°S correspond to areas where precipitation/snowfall excess linked to the storm track dynamics is expected (Fig. 7b,c).

As for present-day climate, the simulated deep water formation in WICE-EXP is also controlled by the thermal density flux. Due to the stronger vertical gradient of temperature in the ocean-atmosphere interface, the thermal density flux anomalies (Fig. 7d) generate substantial changes in the surface density (not shown). An increase in the vertical air-sea temperature contrast, and therefore the loss of heat from the ocean to the atmosphere, leads to strong convective mixing and an enhancement of the SH deep water formation in WICE-EXP.

The total (thermal+haline) density flux anomalies are dominated by changes in the thermal flux. Haline flux anomalies are most important over the 30°-60°S latitudinal belt. These findings serve to highlight the importance of the WAIS for the rate of formation of the SH branch of the MOC, in particular for the formation of the deep water in the Ross/Bellingshausen sea and the southern Atlantic.

Paleoreconstructions focusing on the MIS31 period (e.g. Streng et al. (2011), Scherer et al. (2008)) have shown periodic seaice-free conditions at the time, in particular in the Ross Sea. As demonstrated by Scherer et al. (2008) sea surface temperatures were 3-5°C warmer than present

day. Evaluations of deep-sea sediments recovered at ODP sites 1094 and 1165 (Maiorano et al. (2009), Flores and Sierro (2007)) revealed that the absence of the WAIS leads to a southward displacement of the polar front in the South Atlantic sector. These anomalous patterns indicated by the recontruction are reasonably simulated by our climate model experiments presented here. It should be stressed that the similarities between the modelling results and reconstructions discussed above solely consider the spatial pattern of differences between the MOD and WICE-EXP simulations due to the limitation of the modelling setup in terms of boundary conditions. Thus, our work is not intended to provide a truely realistic account of the reconstructions.

3. Summary and concluding remarks

Through two 1000 years coupled climate simulations of present day and a sensitivity experiment taking into account the reduced WAIS topography, we have demonstrated that changes of the West Antarctic Ice Sheet (WAIS) orography leads to remarkable changes in the oceanic and atmospheric circulations. In the WICE-EXP simulation, the Southern Hemisphere warms by up to 8°C in the polar oceans whereas the Northern Hemsiphere warms by up to 2°C in comparison with the present day climate. Hence, seaice is reduced in the both hemispheres SH. These changes induce a weakening (strengthening) of the extratropical westerlies in the SH (northern Atlantic) in agreement with the thermal wind relation.

Changes in the WAIS also inducea an anomalous pattern of temperature and westerlies associated with SAM. Indeed, a northward shift of the westerly flow and a weakening of the polar jet have been identified. These changes lead to modification in the rate of deep water formation reducing the magnitude of the North Atlantic Deep Water but enhancing the Antarctic Botton Water formation. By evaluating the density flux we argue that the thermal density flux plays the main role for the modification of the meridional overturning circulation. Moreover, the climate anomalies

between the WICE-EXP and the MOD simulations resemble the bipolar seesaw pattern (Broecker (1998)).

One may assume that the magnitude of the idealized ocean's response to fresh water input (as WAIS retreated), compared with the response to mechanical/topographic atmospheric forcing, should be weaker, particularly for changes in the deep water formation. Stouffer et al. (2007) argued that due to the climatological surface winds, which induce surface water northward, fresher sea surface water in the Southern Ocean will be spread into the other ocean basins.

Studies such as Aiken (2008), investigating the role of sea ice in the global climate system, demonstrated that a fresh water forcing equivalent to 100-yr melt of Southern Hemisphere sea ice leads to surface cooling but subsurface warming related to decreased overtuning. It is claimed, however, that those responses are weak, and the initial state recovers over decades. Additional 0.4 Sv of freshwater to the seaice melting experiment also confirms the relatively weak response of the SH to such forcing.

By using a three-dimensional Earth system model of intermediate complexity (EMIC), Swingedouw et al. (2008) argued that the climatic impact of AIS melting is primarily induced by interactions with the ocean and sea ice, and less dependent on fresh water discharge.

The lack of integrated paleoclimate data as well as the absence of astronomical and CO_2 forcing in our experiment, limit the value of a detailed data-model comparison with the MIS31 epoch. The MIS31 interglacial occurred during an extreme peak in astronomical eccentricity that produced very high austral summer insolation anomalies, followed by very intense boreal summers approximately 10,500 yrs later. If accounted for here, this certainly would have impacted the model results. However, generic sensitivity test of the global response to a smaller WAIS, as presented here, have relevance to both past interglacials when WAIS retreated and possibly to the future when the WAIS can be affected by the anthropogenic forcing.

Acknowledgments. We are pleased to acknowledge useful conversations with David Pollard on the subject of this paper and for making available the topography files. The authors would like to thank three anonymous reviewers for their valuable contributions. Research support has been provided through the FAPEMIG grant 551-13 and CNPq 407681.

References

Ackert, R. P., S. Mukhopadhyay, B. R. Parizek, and H. W. Borns, 2007: Ice elevation near the west antarctic ice sheet divide during the last glaciation. *Geophysical Research Letters*, **34 (21)**, n/a–n/a, doi:10.1029/2007GL031412, URL http://dx.doi.org/10.1029/2007GL031412.

Aiken, C. M. M. H. E., 2008: Sensitivity of the present-day climate to freshwater forcing associated with antarctic sea ice loss. *Journal of Climate*, **21**, 3936–3946, doi:10.1175/2007JCLI1901.1.

Broecker, W., 1998: Paleocean circulation during the last deglaciation. A bipolar seesaw? *Paleoceanography*, **13**, 119–121.

Carvalho, L. M. V., C. Jones, and T. Ambrizzi, 2005: Opposite phases of the Antarctic Oscillation and Relationships with Intraseasonal to Interannual activity in the tropics during the Austral Summer. *J.Clim.*, **(18)**, 702–718.

Chan, W.-L., A. Abe-Ouchi, and R. Ohgaito, 2011: Simulating the mid-pliocene climate with the miroc general circulation model: experimental design and initial results. *Geoscientific Model Development*, **4 (4)**, 1035–1049, doi:10.5194/gmd-4-1035-2011, URL http://www.geosci-model-dev.net/4/1035/2011/.

Chapman, W., and J. Walsh, 2007: A synthesis of Antarctic temperatures. *J. Clim.*, **20**, 4096–4117.

Danabasoglu, G., J. C. McWilliams, and W. G. Large, 1996: Approach to equilibrium in accelerated global oceanic models. *Journal of Climate*, **9 (5)**, 1092–1110, doi:10.1175/1520-0442(1996)009⟨1092:ATEIAG⟩2.0.CO;2, URL http://dx.doi.org/10.1175/1520-0442(1996)009⟨1092:ATEIAG⟩2.0.CO;2.

DeConto, R., D. Pollard, and D. Harwood, 2007: Sea ice feedback and Cenozoic evolution of Antarctic climate and ice sheets. *Paleocenography*, **22**, doi:10.1029/2006PA001350.

DeConto, R. M., and D. Pollard, 2003: Rapid Cenozoic glaciation of Antarctica induced by declining atmospheric CO2. *Nature*, doi:10.1038/nature01290.

DeConto, R. M., D. Pollard, and D. Kowalewski, 2012: Modeling antarctic ice sheet and climate variations during marine isotope stage 31. *Global and Planetary Change*, **8889 (0)**, 45 – 52, doi:http://dx.doi.org/10.1016/j.gloplacha.2012.03.003, URL http://www.sciencedirect.com/science/article/pii/S0921818112000434.

Flores, J.-A., and F. J. Sierro, 2007: Pronounced mid-pleistocene southward shift of the polar front in the atlantic sector of the southern ocean. *Deep Sea Research Part II: Topical Studies in Oceanography*, **54 (21)**, 2432 – 2442, doi:http://dx.doi.org/10.1016/j.dsr2.2007.07.026, URL http://www.sciencedirect.com/science/article/pii/S0967064507001816, paleoceanography and Paleoclimatology of the Southern Ocean A Synthesis of Three Decades of Scientific Ocean Drilling.

Goldner, A., M. Huber, and R. Caballero, 2013: Does antarctic glaciation cool the world? *Climate of the Past*, **9 (1)**, 173–189, doi:10.5194/cp-9-173-2013, URL http://www.clim-past.net/9/173/2013/.

Goosse, H., and T. Fichefet, 1999: Importance of ice-ocean interactions for the global ocean circulation: a model study. *J. Geophys. Res.*, **104(C10)**, 23 337–23 355.

Hamon, N., P. Sepulchre, Y. Donnadieu, A.-J. Henrot, L. Franois, J.-J. Jaeger, and G. Ramstein, 2012: Growth of subtropical forests in miocene europe: The roles of carbon dioxide and antarctic ice volume. *Geology*, **40 (6)**, 567–570, doi:10.1130/G32990.1, URL http://geology.gsapubs.org/content/40/6/567.abstract, http://geology.gsapubs.org/content/40/6/567.full.pdf+html.

Haywood, A. M., M. A. Chandler, P. J. Valdes, U. Salzmann, D. J. Lunt, and H. J. Dowsett, 2009: Comparison of mid-pliocene climate predictions produced by the hadam3 and {GCMAM3} general circulation models. *Global and Planetary Change*, **66 (34)**, 208 – 224, doi:http://dx.doi.org/10.1016/j.gloplacha.2008.12.014, URL http://www.sciencedirect.com/science/article/pii/S0921818108002142.

Haywood, A. M., and Coauthors, 2010: Pliocene model intercomparison project (pliomip): experimental design and boundary conditions (experiment 1). *Geoscientific Model Development*, **3 (1)**, 227–242, doi:10.5194/gmd-3-227-2010, URL http://www.geosci-model-dev.net/3/227/2010/.

Holden, P. B., N. R. Edwards, E. W. Wolff, N. J. Lang, J. S. Singarayer, P. J. Valdes, and T. F. Stocker, 2010: Interhemispheric coupling, the west antarctic ice sheet and warm antarctic interglacials. *Climate of the Past*, **6 (4)**, 431–443, doi:10.5194/cp-6-431-2010, URL http://www.clim-past.net/6/431/2010/.

Hosking, J. S., A. Orr, M. J. Gareth, J. Turner, and T. Philips, 2013: Energy and numerical weather prediction. *J. Climate*, **26**, 6633–6648, doi:10.1175/JCLIM-D-12-00813.1.

Justino, F., J. Marengo, F. Kucharski, F. Stordal, J. Machado, and M. Rodrigues, 2014: Influence of antarctic ice sheet lowering on the southern hemisphere climate: modeling experiments

mimicking the mid-miocene. *Climate Dynamics*, 1–16, doi:10.1007/s00382-013-1689-9, URL http://dx.doi.org/10.1007/s00382-013-1689-9.

Justino, F., and W. Peltier, 2006: Influence of Present Day and Glacial Surface Conditions on the Antarctic Oscillation/Southern Annular Mode. *Geophys. Res. Lett.*, doi:10.1029/2006GL027001.

Justino, F., and W. R. Peltier, 2005: The glacial North Atlantic Oscillation. *Geophys. Res. Lett.*, **32**, L21 803, doi:10.1029/2005GL023822.

Justino, F., A. Setzer, T. J. Bracegirdle, D. Mendes, A. Grimm, G. Dechiche, and C. E. G. R. Schaefer, 2010: Harmonic analysis of climatological temperature over Antarctica: present day and greenhouse warming perspectives. *Internation Journal of Climatology*, doi: 10.1002/joc.2090.

Kageyama, M., and P. Valdes, 2000: Impact of the north american ice-sheet orography on the last glacial maximum eddies and snowfall. *Geophys. Res. Lett.*, **27 (10)**, 1515–1518.

Knorr, G., and G. Lohmann, 2014: Climate warming during antarctic ice sheet expansion at the middle miocene transition. *Nature Geoscience*, **7**, 376–381, doi:10.1038/ngeo2119.

Knutti, R., J. Flueckiger, T. Stocker, and A. Timmermann, 2004: Strong hemispheric coupling of glacial climate through continental freshwater discharge and ocean circulation. *Nature*, **430**, 851–856.

Kucharski, F., F. Molteni, and A. Bracco, 2006: Decadal interactions between the western tropical Pacific and the North Atlantic Oscillation. *Clim. Dyn.*, **26**, 79–91.

Lefebvre, W., H. Goosse, R. Timmermann, and T. Fichefet, 2004: Influence of the Southern Annular Mode on the sea ice-ocean system. *J. Geophys. Res.*, **109**, doi:10.1029/2004JC002403.

L'Heureux, M. L., and D. W. J. Thompson, 2006: Observed Relationships between the El Niño Southern Oscillation and the Extratropical Zonal-Mean Circulation. *J. Clim.*, **19 (2)**, 276–287.

Maiorano, P., M. Marino, and J.-A. Flores, 2009: The warm interglacial marine isotope stage 31: Evidences from the calcareous nannofossil assemblages at site 1090 (southern ocean). *Marine Micropaleontology*, **71 (34)**, 166 – 175, doi:http://dx.doi.org/10.1016/j.marmicro.2009.03.002, URL http://www.sciencedirect.com/science/article/pii/S0377839809000255.

Manabe, S., and R. J. Stouffer, 1995: Simulation of abrupt climate change induced by freshwater input to the North Atlantic Ocean. *Nature*, **378**, 165–167.

Marshall, J., and K. Speer, 2012: Closure of the meridional overturning circulation through southern ocean upwelling. *Nature Geoscience*, **5**, 1710–180.

Mellor, G., and T. Yamada, 1982: Development of a turbulence closure model for geophysical fluid problems. *Rev. Geophys. Space Phys.*, **20**, 851–875.

Munneke, P., Kuipers, M. R. van den Broeke, J. T. M. Lenaerts, M. G. Flanner, A. S. Gardner, and W. J. van de Berg, 2011: A new albedo parameterization for use in climate models over the antarctic ice sheet. *Journal of Geophysical Research: Atmospheres*, **116 (D5)**, n/a–n/a, doi: 10.1029/2010JD015113, URL http://dx.doi.org/10.1029/2010JD015113.

Naish, T., and Coauthors, 2009: Obliquity-paced pliocene west antarctic ice sheet oscillations. *Nature*, **458 (7236)**, 322–328, URL http://www.scopus.com/inward/record.url?eid=2-s2.0-62649146401&partnerID=40&md5=4e09abf599f8dff4361f5ce5927d7648, cited By (since 1996)177.

Pekar, S. F., and R. M. DeConto, 2006: High-resolution ice-volume estimates for the early miocene: Evidence for a dynamic ice sheet in antarctica. *Palaeogeography, Palaeoclimatol-*

561 *ogy, Palaeoecology*, **231 (12)**, 101–109, doi:10.1016/j.palaeo.2005.07.027, URL http://www.
562 sciencedirect.com/science/article/pii/S0031018205004839.

563 Peltier, W., 2004: Global glacial isostasy and the surface of the ice-age Earth: the ICE-5G (VM2)
564 model and GRACE. *Annual Review of Earth and Planetary Sciences.*, **32**, 111–149.

565 Pollard, D., and R. DeConto, 2009: Modelling west antarctic ice sheet growth and collapse through
566 the past five million years. *Nature*, http://dx.doi.org/10.1038/nature07809.

567 Pollard, D., and R. M. DeConto, 2005: Hysteresis in cenozoic antarctic ice-sheet variations.
568 *Global and Planetary Change*, **45**, 9 – 21, doi:10.1016/j.gloplacha.2004.09.011, URL http:
569 //www.sciencedirect.com/science/article/pii/S0921818104001377, ¡ce:title¿Long-term changes
570 in Southern high-latitude ice sheets and climate, the Cenozoic history¡/ce:title¿.

571 Pollard, D., R. M. DeConto, and A. A. Nyblade, 2005: Sensitivity of cenozoic antarc-
572 tic ice sheet variations to geothermal heat flux. *Global and Planetary Change*, **49**, 63 –
573 74, doi:10.1016/j.gloplacha.2005.05.003, URL http://www.sciencedirect.com/science/article/
574 pii/S0921818105001049.

575 Rahmstorf, S., 1996: On the freshwater forcing and transport of the atlantic thermohaline circula-
576 tion. *Climate Dynamics*, **4**, 73–79.

577 Scherer, R. P., and Coauthors, 2008: Antarctic records of precession-paced insolation-driven
578 warming during early pleistocene marine isotope stage 31. *Geophysical Research Letters*, **35 (3)**,
579 doi:10.1029/2007GL032254, URL http://dx.doi.org/10.1029/2007GL032254.

580 Schmitt, R., P. Bogden, and C. Dorman, 1989: Evaporation minus precipitation and density flux
581 for the North Atlantic. *J. Phys. Oceanogr.*, **(19)**, 1208–1221.

582 Severijns, C. A., and W. Hazeleger, 2010: The efficient global primitive equation climate model
583 SPEEDO V2.0. *Geosci. Model Dev.*, **3**, 105–122, doi:10.5194/gmd-3-105-2010.

584 Speer, K., S. R. Rintoul, and B. Sloyan, 2000: The diabatic deacon cell. *J. Phys. Oceanogr.*, **30**.

585 Speer, K., and E. Tziperman, 1992: Rates of water mass formation in the North Atlantic Ocean. *J.*
586 *Phys. Oceanogr.*, **22**, 94–104.

587 Stouffer, R., D. Seidov, and B. Haupt, 2007: Climate Response to External Sources of Freshwater:
588 North Atlantic versus the Southern Ocean. *J. Climate*, **20**, 436–448.

589 Streng, M., O. Esper, and J. Wollenburg, 2011: Calcareous dinoflagellate cysts from
590 the pleistocene (marine isotope stage 31) of the ross sea, antarctica. *Antarctic Science*,
591 **23**, 597–604, doi:10.1017/S0954102011000605, URL http://journals.cambridge.org/article_
592 S0954102011000605.

593 Swingedouw, D., T. Fichefet, P. Huybrechts, H. Goosse, E. Driesschaert, and M.-F. Loutre, 2008:
594 Antarctic ice-sheet melting provides negative feedbacks on future climate warming. *Geophysi-*
595 *cal Research Letters*, **35 (17)**, n/a–n/a, doi:10.1029/2008GL034410, URL http://dx.doi.org/10.
596 1029/2008GL034410.

597 Whitehouse, P. L., M. J. Bentley, and A. M. L. Brocq, 2012: A deglacial model for antarc-
598 tica: geological constraints and glaciological modelling as a basis for a new model of
599 antarctic glacial isostatic adjustment. *Quaternary Science Reviews*, **32 (0)**, 1 – 24, doi:
600 http://dx.doi.org/10.1016/j.quascirev.2011.11.016, URL http://www.sciencedirect.com/science/
601 article/pii/S0277379111003726.

602 Zachos, J., M. Pagani, L. Sloan, E. Thomas, and K. Billups, 2001: Trends, Rhythms, and Aberra-
603 tions in Global Climate 65 Ma to Present. *Science*, dOI:10.1126/science.1059412.

Zhang, Z. S., and Coauthors, 2012: Pre-industrial and mid-pliocene simulations with noresm-l. *Geoscientific Model Development*, **5 (2)**, 523–533, doi:10.5194/gmd-5-523-2012, URL http://www.geosci-model-dev.net/5/523/2012/.

LIST OF FIGURES

Fig. 1. Present day topography (a), WICE-EXP topography (b) and the differences between the WICE-EXP and MOD simulation (c). The unit is meter 30

Fig. 2. (a) Amplitude of the first harmonic of the near surface air temperature [°C], (b,c) is the amplitude for precipitation [mm/day] and the zonal winds [m/s] at 850 hPa for MOD simulation. (d, e and f) is the same but for the NNR1 and GPCP datasets 31

Fig. 3. (a) Zonally averaged precipitation [mm/day] and (b) near surface air temperature [°C]. The black (red) line is for MOD simulation (GPCP and NNR1) 32

Fig. 4. (a) Annually averaged near surface temperature (°C) for the MOD simulation and (b) is the differences between the WICE-EXP and MOD simulations. (c) and (d) are the same but for zonal winds, (e) and (f) are the same as in (a) and (b) but for the geopotential height at 700hPa [meters]. (g) and (h) are the same as in (e) and (f) but for precipitation (mm/day). Dotted regions are statistically significant at 95% level based on student t-test. 33

Fig. 5. (a) Z700 [m], (b) near surface temperature [°C], (c) near zonal wind (m/s) response associated with the positive phase of Southern Annular Mode in the MOD simulation. (d), (e) and (f) show differences between the WICE-EXP and MOD simulations. The patterns are displayed as amplitudes by regressing hemispheric climate anomalies upon the standardized first principal component time series. Please note that figures are shown with different labels. . 34

Fig. 6. Annually averaged sea surface temperature (SST, °C) for the MOD simulation and (b) the differences between the WICE-EXP and MOD simulations. (c) Annually averaged seaice thickness for MOD, and (d) is the differences between the WICE-EXP and MOD simulations. Dotted regions are statistically significant at 95% level based on student t-test. (e) is the all-basin annually zonally averaged vertical ocean temperatures differences between the WICE-EXP and the MOD simulation. (f) is the same as (e) but averaged only in the Atlantic basin. 35

Fig. 7. (a) Meridional overturning circulation for the MOD simulation, global ocean (shaded) and the Atlantic (contour). b) is the differences between the WICE-EXP and MOD simulations (a). Annually averaged annual density flux in MOD [$10^{-6} \times kgm^{-2}s^{-1}$]. (c) thermal contribution, (d) haline contribution and (e) thermal+haline. (f), (g) and (h) the same as a,b,c but for the differences between the WICE-EXP and the MOD simulation. 36

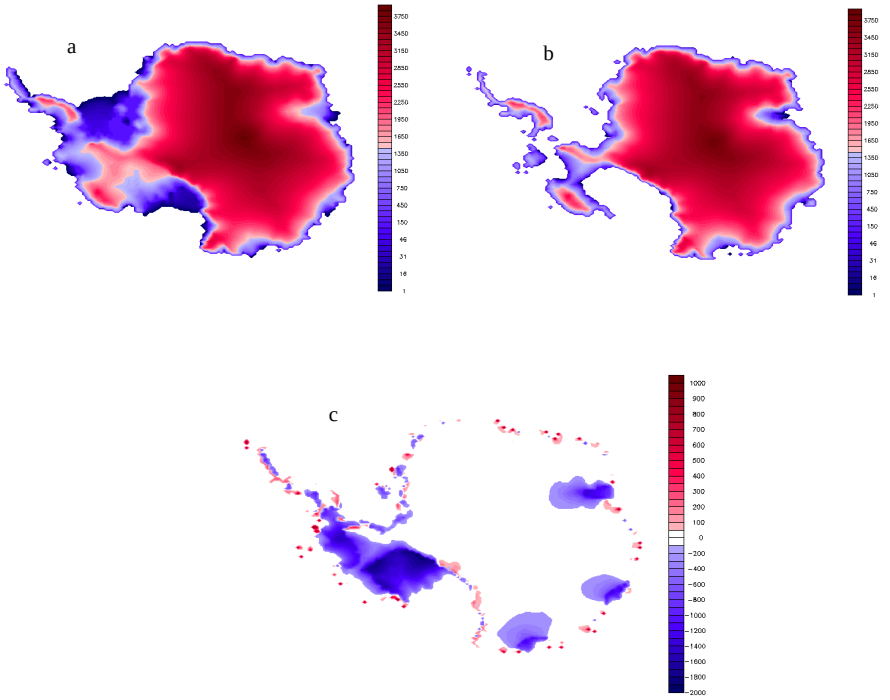

FIG. 1. Present day topography (a), WICE-EXP topography (b) and the differences between the WICE-EXP and MOD simulation (c). The unit is meter

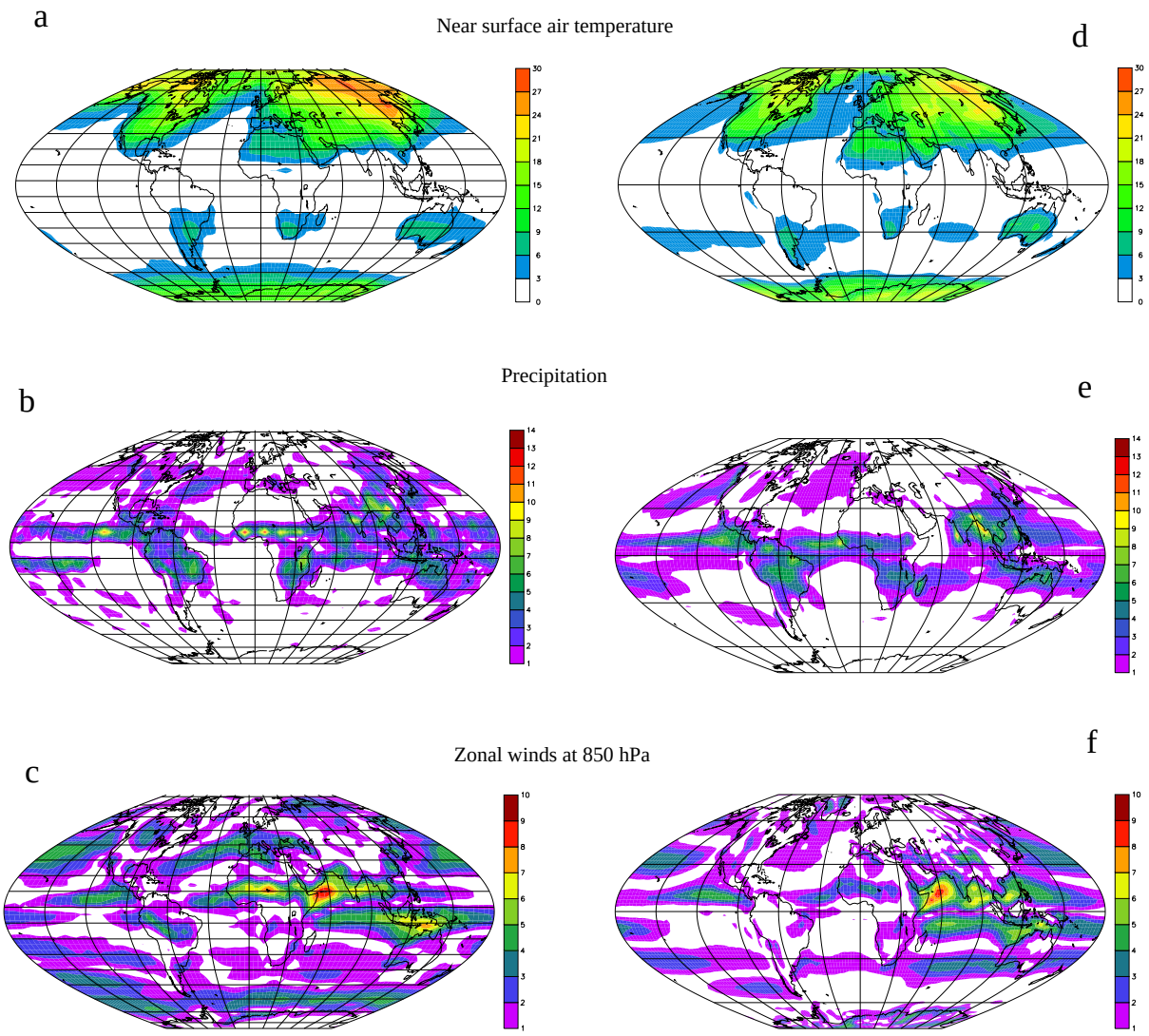

639 FIG. 2. (a) Amplitude of the first harmonic of the near surface air temperature [°C], (b,c) is the amplitude for
640 precipitation [mm/day] and the zonal winds [m/s] at 850 hPa for MOD simulation. (d, e and f) is the same but
641 for the NNR1 and GPCP datasets

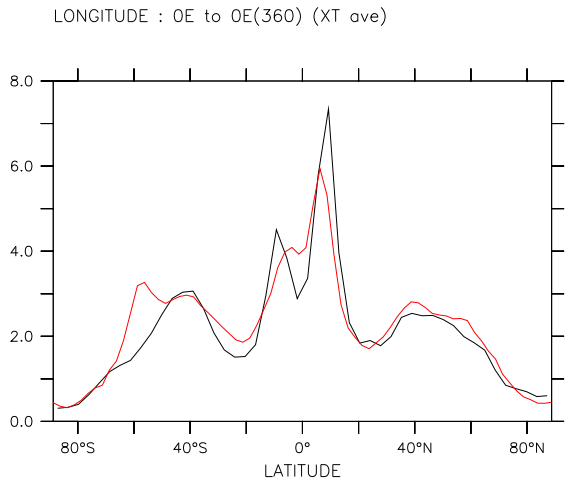

a) Precipitation – Zonal Mean (mm/day)

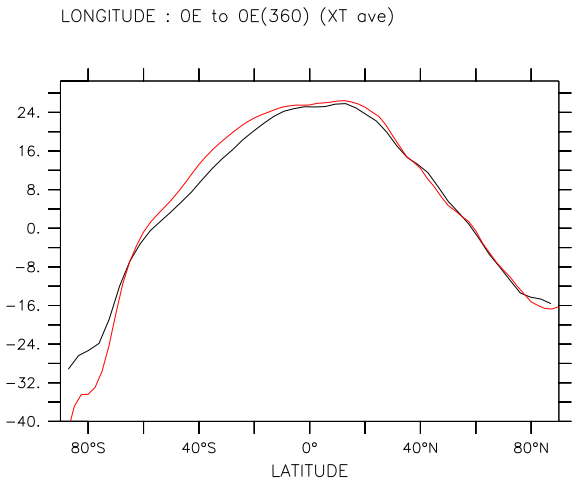

b) Near Surface Temperature – Zonal Mean (C)

642 FIG. 3. (a) Zonally averaged precipitation [mm/day] and (b) near surface air temperature [°C]. The black (red)
643 line is for MOD simulation (GPCP and NNR1)

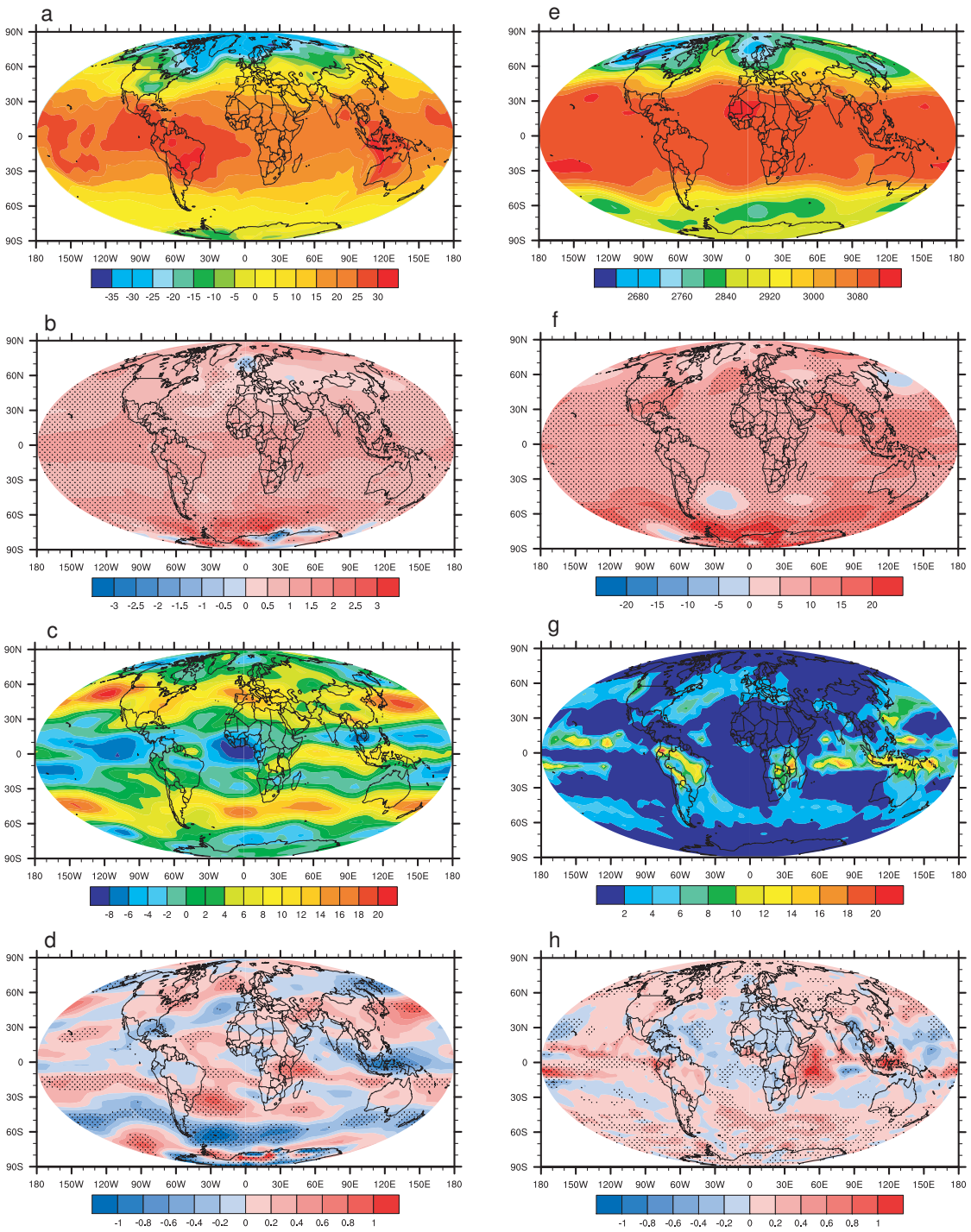

644 FIG. 4. (a) Annually averaged near surface temperature (°C) for the MOD simulation and (b) is the differences
645 between the WICE-EXP and MOD simulations. (c) and (d) are the same but for zonal winds, (e) and (f) are the
646 same as in (a) and (b) but for the geopotential height at 700hPa [meters]. (g) and (h) are the same as in (e) and (f)
647 but for precipitation (mm/day). Dotted regions are statistically significant at 95% level based on student t-test.

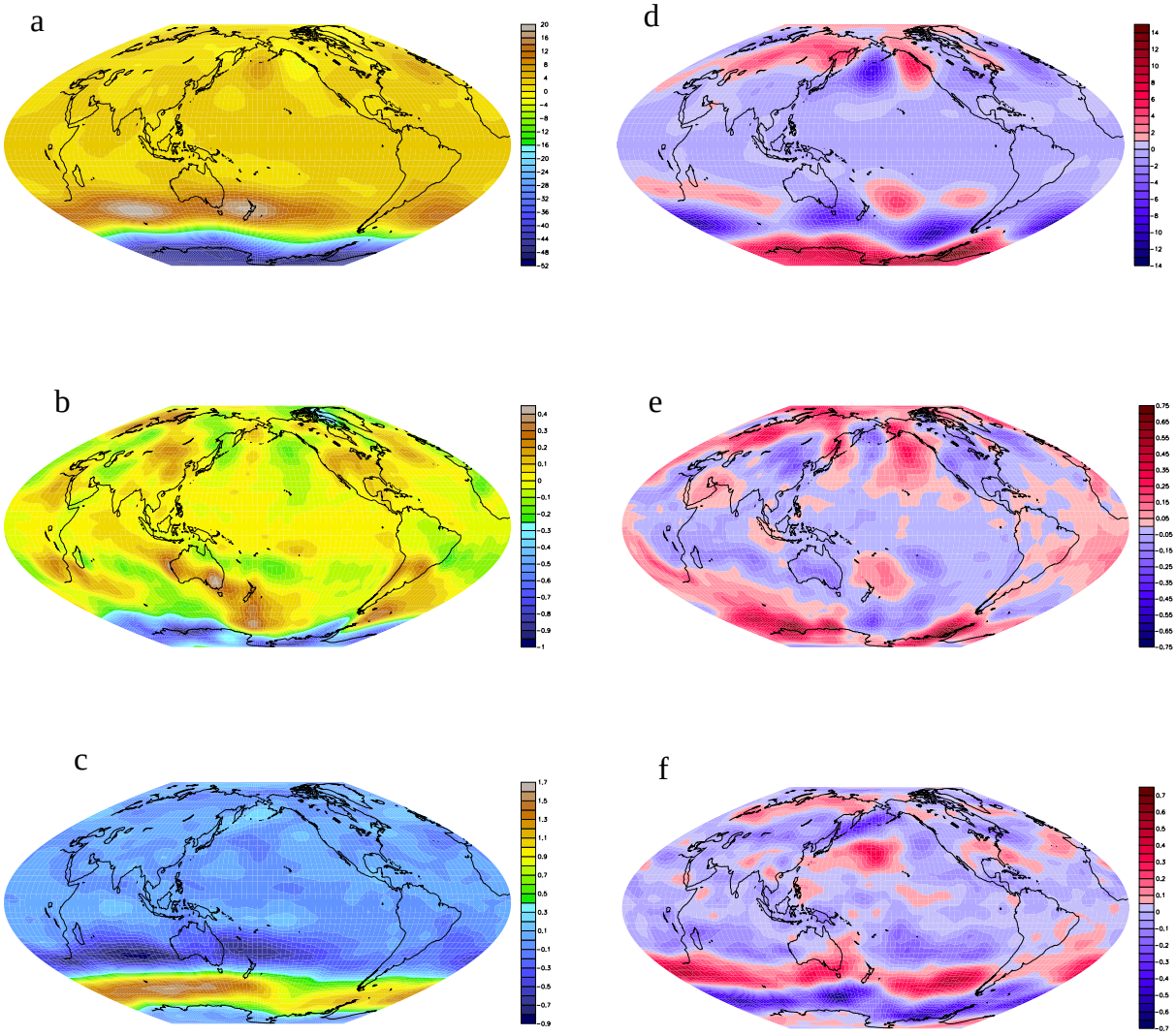

FIG. 5. (a) Z700 [m], (b) near surface temperature [°C], (c) near zonal wind (m/s) response associated with the positive phase of Southern Annular Mode in the MOD simulation. (d), (e) and (f) show differences between the WICE-EXP and MOD simulations. The patterns are displayed as amplitudes by regressing hemispheric climate anomalies upon the standardized first principal component time series. Please note that figures are shown with different labels.

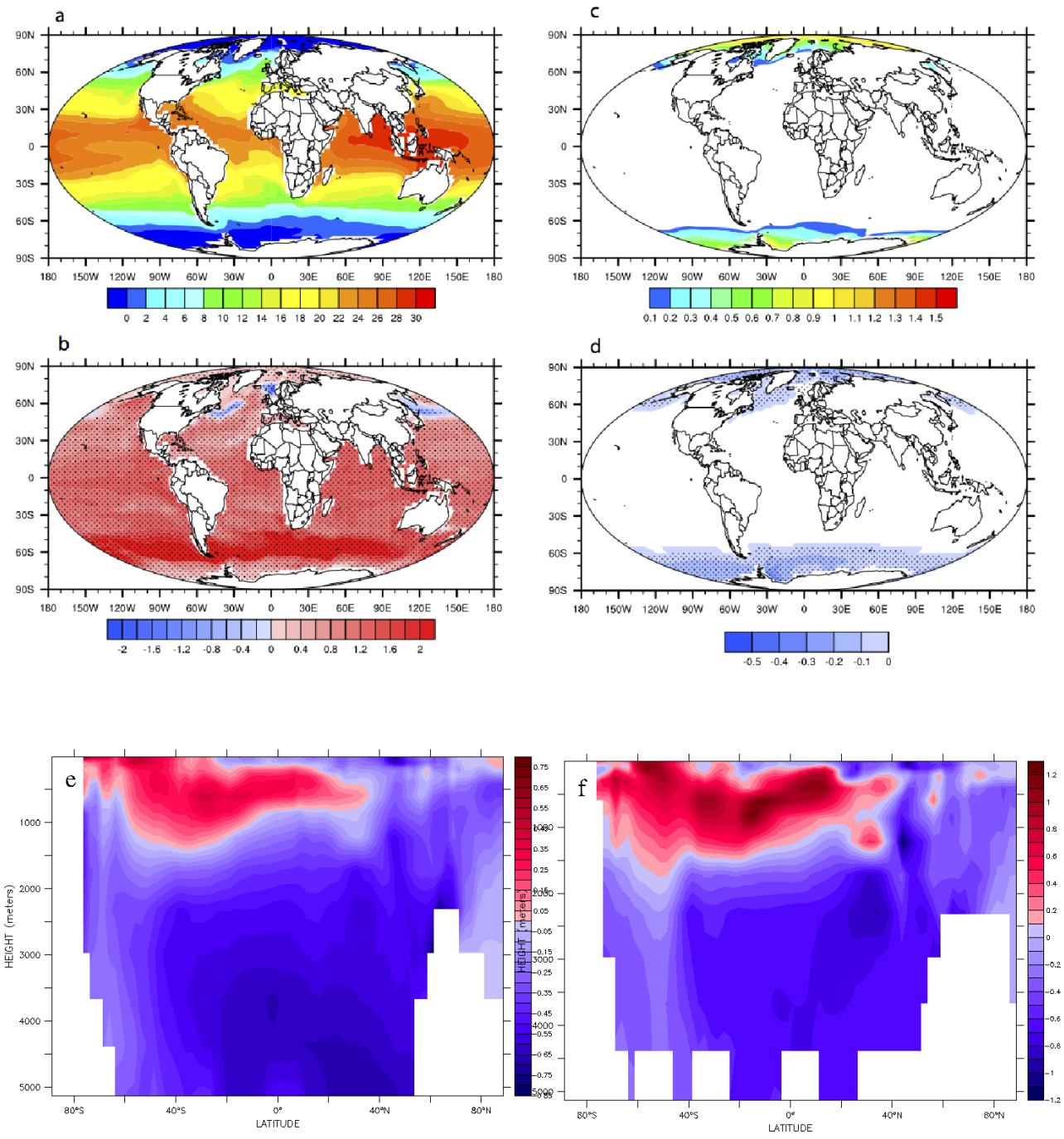

653 FIG. 6. Annually averaged sea surface temperature (SST, °C) for the MOD simulation and (b) the differences
654 between the WICE-EXP and MOD simulations. (c) Annually averaged seaice thickness for MOD, and (d) is
655 the differences between the WICE-EXP and MOD simulations. Dotted regions are statistically significant at
656 95% level based on student t-test. (e) is the all-basin annually zonally averaged vertical ocean temperatures
657 differences between the WICE-EXP and the MOD simulation. (f) is the same as (e) but averaged only in the
658 Atlantic basin.

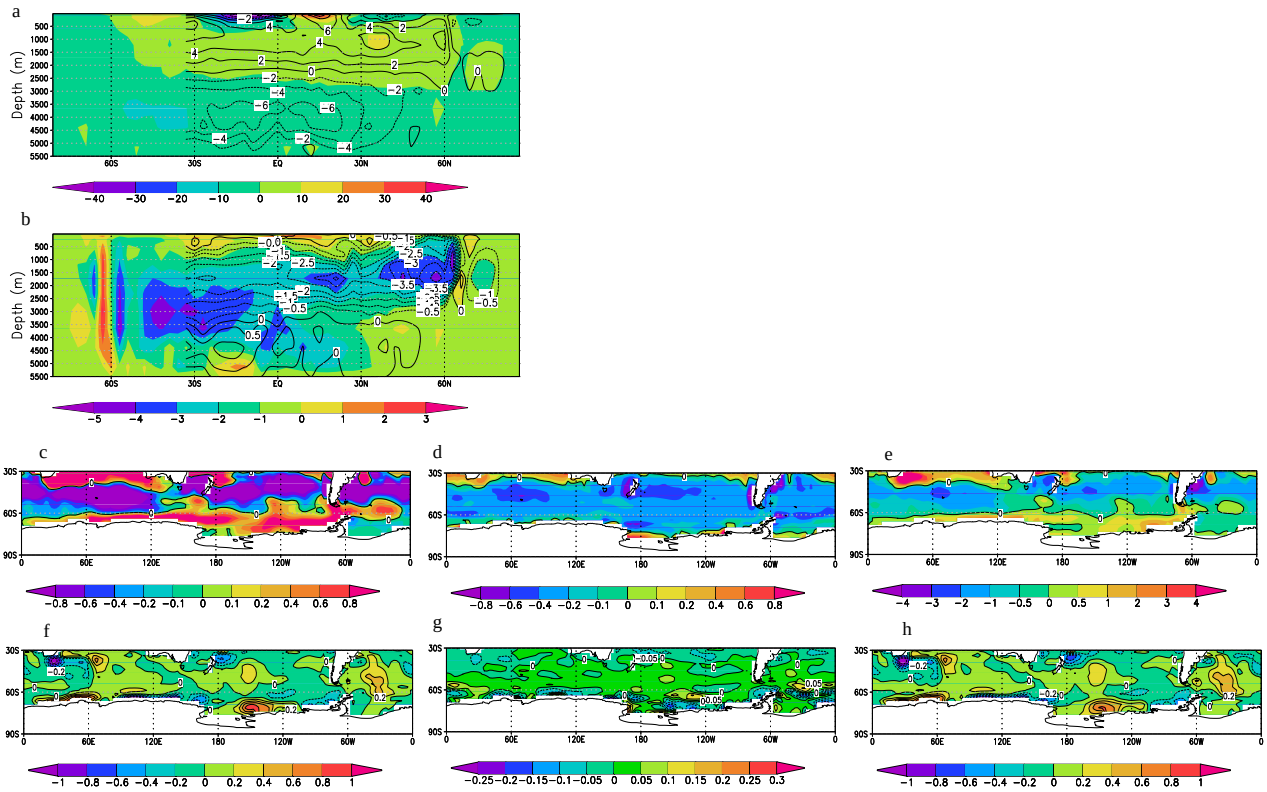

FIG. 7. (a) Meridional overturning circulation for the MOD simulation, global ocean (shaded) and the Atlantic (contour). b) is the differences between the WICE-EXP and MOD simulations (a). Annually averaged annual density flux in MOD $[10^{-6} \times kgm^{-2}s^{-1}]$. (c) thermal contribution, (d) haline contribution and (e) thermal+haline. (f), (g) and (h) the same as a,b,c but for the differences between the WICE-EXP and the MOD simulation.